BEC BIOENERGETICS COMMUNICATIONS
Bioenerg Commun 2021.3
doi:10.26124/bec:2021-0003
Open Access

Technical Communication

Cite
Komlódi T, Cardoso LHD, Doerrier C, Moore AL, Rich PR, Gnaiger E (2021) Coupling and pathway control of coenzyme Q redox state and respiration in isolated mitochondria. Bioenerg Commun 2021.3. doi:10.26124/bec:2021-0003

Author contributions
EG and TK collaborated closely with WGT in the development of the Q-Module, with guidance from ALM and PRR. TK and LHDC designed, carried out and analyzed the experiments. CD contributed to SUIT protocol development. TK, LHDC and EG co-wrote the manuscript. All authors commented on and approved the manuscript.

Conflicts of interest
EG is founder and CEO of Oroboros Instruments, Innsbruck, Austria.

Academic editor
Alicia J Kowaltowski, University of Sao Paulo, BR

Copy editor
Lisa Tindle-Solomon

Received 2021-09-15
Reviewed 2021-10-13
Resubmitted 2021-11-09
Accepted 2021-11-09

Published 2021-11-11

Editorial and peer review record
doi:10.26124/bec:2021-0003

Preprint
MitoFit Preprints 2021.2.v4
doi:10.26124/mitofit:2021-0002.v4

Coupling and pathway control of coenzyme Q redox state and respiration in isolated mitochondria

Timea Komlódi[1], Luiza HD Cardoso[1], Carolina Doerrier[1], Anthony L Moore[2], Peter R Rich[3], Erich Gnaiger[1]*

[1] Oroboros Instruments, Innsbruck, Austria;
[2] Biochemistry and Medicine, School of Life Sciences, Univ Sussex, Falmer, Brighton, UK;
[3] Dept Structural and Molecular Biol, Univ College London, London, UK

* Corresponding author: erich.gnaiger@oroboros.at

Abstract

Redox states of the mitochondrial coenzyme Q pool, which reacts with the electron transfer system, reflect the balance between (*1*) reducing capacities of electron flow from fuel substrates converging at the Q-junction, (*2*) oxidative capacities downstream of Q to O_2, and (*3*) the load on the OXPHOS system utilizing or dissipating the protonmotive force.

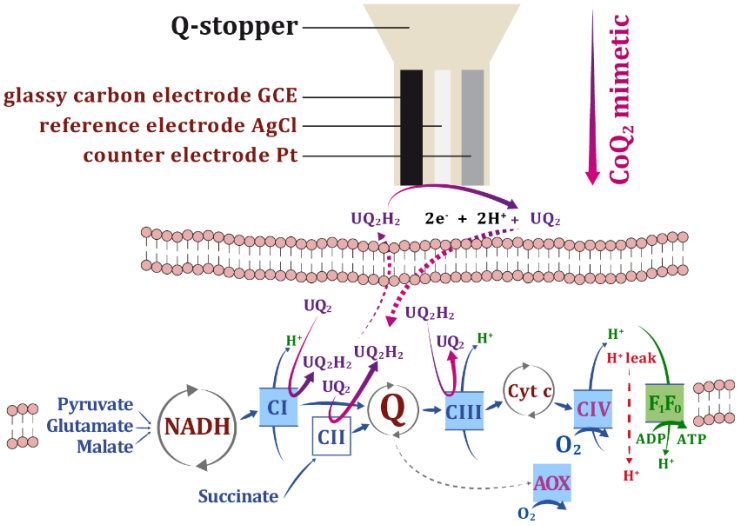

Data availability
Original files are available Open Access at Zenodo repository:
10.5281/zenodo.4478400

Keywords
coenzyme Q, CoQ
Q-junction
Q-redox state
electron transfer system, ETS
ETS-reactive Q-pool, Q
mitochondrial coenzyme Q, mtCoQ
supercomplexed Q
free Q-pool according to the fluid-state model, Q_{free}
cyclic voltammetry, CV
high-resolution respirometry, HRR
isolated mitochondria, imt
mouse heart mitochondria
mouse brain mitochondria
oxygen consumption
SUIT protocols
coupling control
pathway control
NS-pathway
additivity

A three-electrode sensor (Rich 1988; Moore et al 1988) was implemented into the NextGen-O2k to monitor continuously the redox state of CoQ_2 added as a Q-mimetic simultaneously with O_2 consumption. The Q-Module was optimized for high signal-to-noise ratio, minimum drift, and minimum oxygen diffusion. CoQ_2 equilibrates in the same manner as Q at Complexes CI, CII and CIII. The CoQ_2 redox state is monitored amperometrically with the working electrode, which is poised at CoQ_2 redox peak potentials determined by cyclic voltammetry. The voltammogram also provides quality control of the Q-sensor and reveals chemical interferences.

The CoQ_2 redox state and O_2 consumption were measured simultaneously in isolated mouse cardiac and brain mitochondria. CoQ_2 — and by implication mitochondrial Q — was more oxidized when O_2 flux was stimulated by coupling control: when energy demand increased from LEAK to OXPHOS and electron transfer capacities in the succinate pathway. In contrast, CoQ_2 was more reduced when O_2 flux was stimulated by pathway-control of electron input capacities, increasing from the NADH (N)- to succinate (S)-linked pathway which converge at the Q-junction, with CI-Q-CIII and CII-Q-CIII segments, respectively. N- and S-respiratory pathway capacities were not completely additive, compatible with partitioning of Q intermediary between the solid-state and liquid-state models of supercomplex organization. The direct proportionality of CoQ_2 reduction and electron input capacities through the CI-Q-CIII and CII-Q-CIII segments suggests that CoQ_2 is accurately mimicking mitochondrial Q-redox changes.

1. Introduction

The redox state of mitochondrial metabolites plays a key role in mitochondrial respiratory control. Analysis of O_2 consumption is one of the most established methods to study mitochondrial function in health and disease. High-resolution respirometry (HRR) is a state-of the art technique to measure mitochondrial respiration in a wide variety of sample preparations with the application of substrate-uncoupler-inhibitor titration (SUIT) protocols (Doerrier et al 2018). Extensions of HRR in the Oroboros Oxygraph-2k (O2k, Oroboros Instruments, Innsbruck, Austria) by fluorometric or potentiometric modules allow simultaneous measurements of respiration and additional

mitochondrial parameters (e.g. mitochondrial membrane potential, ATP synthesis, hydrogen peroxide production, Ca^{2+}, pH, NO, H_2S). The Oroboros NextGen-O2k is a novel all-in-one instrument which extends HRR with the amperometric measurement of the redox state of a Q-mimetic, such as CoQ_2, added to the experimental chamber. The Q-mimetic equilibrates with the part of the mitochondrial coenzyme Q-pool which reacts with the electron transfer system (ETS-reactive Q). Thus, pivotal information is obtained on the relation between Q-redox state and electron transfer at controlled O_2 regimes in the range of hyperoxia to anoxia, whilst saving resources (time, biological sample, and reagents), and ensuring reproducibility and accuracy of the results. Importantly, mitochondrial coenzyme Q-redox states are not measured directly, but the signal is indirect and mediated by the Q-mimetic.

Mitochondrial coenzyme Q (mtCoQ; ubiquinone; 2,3-dimethoxy-5-methyl-6-polyprenyl-1,4-benzoquinone) was discovered in 1957 by Crane and colleagues. CoQ occurs in mitochondrial and other cellular membranes. It is a lipid composed of a benzoquinone ring with an isoprenoid side chain, two methoxy groups and one methyl group (Wolf et al 1958). The number *N* of isoprenoid units is indicated as CoQ_N (ChEBI ontology; https://www.ebi.ac.uk/chebi/chebiOntology.do?chebiId=CHEBI:46245). For example, CoQ_8 occurs in *Trypanosoma brucei*, CoQ_9 in *Caenorhabditis elegans* and rodents, CoQ_{10} in humans. Some species have more than one CoQ form, e.g. human and rodent mitochondria contain different proportions of CoQ_9 and CoQ_{10} (Aberg et al 1992; Awad et al 2018; Hernández-Camacho et al 2018; Watts, Ristow 2017).

CoQ is endogenously synthesized in all mammalian cells and absorption of CoQ from the diet is limited (Miles 2007). The isoprenoid side chain is synthetized through the mevalonate-pathway from acetyl-CoA (Goldstein, Brown 1990; Bentinger et al 2010). For further details on the CoQ biosynthesis, see: Tran, Clarke 2007; Kalén et al 1987; Stefely, Pagliarini 2017; González-Mariscal et al 2014. Currently nine genes are known to be involved in endogenous CoQ_{10} (human) or CoQ_6 (yeast) biosynthesis (Alcázar-Fabra et al 2016; Gvozdjakova et al 2021; Tran, Clarke 2007). Mutation of these genes or degradation of CoQ_{10} leads to lower levels of CoQ_{10} associated with several diseases (Fazakerley et al 2018; Gvozdjakova et al 2020).

CoQ is widely distributed among non-mitochondrial compartments. In hepatocytes CoQ localizes in the Golgi apparatus (Crane et al 1985; Nyquist et al 1970), peroxisomes (Turunen et al 2004), microsomes (Seshadri Sastry et al 1961), and the plasma membrane electron transfer system (review: Morré, Morré 2011). >30 % of the membrane-bound CoQ is extramitochondrial in rat liver (Kalén et al 1987; Morré, Morré 1989). Additionally, lysosomes have an ETS comparable to mitochondria where CoQ acts as an electron carrier (Gille, Nohl 2000). Consequently, isolated mitochondria may be considered as the gold standard for selective measurement of the mitochondrial Q-redox state.

Q is a central component of the mtETS (Crane et al 1959; Hatefi et al 1959, Mitchell 1961) and is involved in antioxidant defense (Noh et al 2013), mitophagy (Rodríguez-Hernández et al 2009), and regulation of permeability transition (Balaban et al 2005; Bentinger et al 2007; Fontaine et al 1998; Lopez-Lluch et al 2010). Several branches of the ETS converge at the Q-junction: In mammalian mitochondria, ETS-reactive Q (redox

active, Q_{ra}; Kröger, Klingenberg 1973a) is reduced by electron supply from (*1*) Complex I (CI), (*2*) CII, (*3*) electron-transferring flavoprotein Complex, (*4*) mt-glycerophosphate dehydrogenase Complex, (*5*) dihydro-orotate dehydrogenase Complex, and from other enzyme complexes (Enriquez, Lenaz 2014; Gnaiger 2020). Q_{ra} is oxidized downstream through CIII. Electrons are subsequentially transferred via cytochrome *c* to CIV and the terminal electron acceptor O_2.

The concept of the Q-cycle was proposed originally by Mitchell (1975) and was elaborated further in several modifications, describing how CIII translocates hydrogen ions against the protonmotive force *pmF* (Mitchell 1961, 1975; Rich 1984; Trumpower 1990; Trumpower, Gennis 1994; Crofts 2004). CoQ refers to all protonation states and the three redox states: ubiquinone (UQ, oxidized), ubiquinol (UQH_2, reduced), and an intermediate free radical semiquinone ($USQ^{\bullet-}$; Song, Buettner 2011). UQH_2 binds to the Q_o site of CIII, while ubiquinone UQ binds to the Q_i site of CIII. First, UQH_2 reduces the iron-sulfur protein and loads cytochrome c_1 with one electron. The other electron is transferred to the b_L heme and reduces the b_H heme, which transfers the electron to UQ at the Q_i site, reducing it to $USQ^{\bullet-}$. A second UQH_2 — oxidized at the Q_o site — is required to fully reduce this semiquinone to ubiquinol UQH_2 at the Q_i site. This results in two UQH_2 oxidized at the Q_o site per one UQ reduced at the Q_i site. In a full Q-cycle, two H^+ leave the mt-matrix, and four H^+ enter the intermembrane space with a change of two net transmembrane charges. The reduced cytochrome *c* transfers electrons further to CIV. The ubiquinol generated at the Q_i site is recycled by binding to the Q_o site of CIII (Hunte et al 2003; Trumpower 1990; Trumpower, Gennis 1994).

Kröger and Klingenberg analyzed the kinetic control of the Q-redox state in submitochondrial particles. An ETS-reactive Q-pool Q_{ra} is distinguished from an inactive pool $mtCoQ_{ia}$. At steady state the redox state of Q_{ra} is proportional to respiratory rate and Q_{ra} has been considered to be homogenous, characterized as Q-pool behavior (Kröger, Klingenberg 1966, 1973a, 1973b; Ernster et al 1969; Hackenbrock et al 1986). However, according to Gutman (1985) there is inhomogeneity of the Q_{ra}-pool with different redox states of Q at various reduction sites (Cottingham, Moore 1983). A third Q-pool is suggested as an exo-mtCoQ-pool, reduced by NADH added to intact pigeon heart mitochondria and located on the outer face of the mtIM (Jørgensen et al 1985). Considering that lateral diffusion of Q is high in the lipid bilayer and not rate-limiting for electron transfer, the inhomogeneity can be explained by $SCI_nIII_nIV_n$ supercomplex formation (NADH oxidation through the CI-Q-CIII branch) in contrast to homogenous 'Q-pool behavior' between CII (and other dehydrogenases) and CIII (succinate oxidation; Bianchi et al 2004; Estornell et al 1992; Rauchová et al 1997; Stoner et al 1984; Enriquez, Lenaz 2014). According to the solid-state model (Rich 1984), Q-intermediates are transferred in currently considered supercomplexes Q_{SC} by substrate channeling preventing equilibration with the free Q-pool Q_{free}. The Q_{free}-pool is a reservoir for slow binding to $SCI_nIII_nIV_n$ and uncoupling proteins (Bianchi et al 2003; Echtay et al 2000; Lenaz, Genova 2009). The solid-state and liquid-state (random-collision) models describe the extremes of a dynamic molecular organization, with intermediary behavior possible depending on factors such as kinetic or physical limitations (Rich 1984) leading to the plasticity model (Enriquez, Lenaz 2014).

Q-extraction is an established method for measurement of the redox state not only of the ETS-reactive Q-pool but also of the inactive mtCoQ-pool, involving extraction and determination of the total concentration of reduced quinol and oxidized quinone by high-performance liquid chromatography (Reed, Ragan 1987; Takada et al 1984; Zannoni, Moore 1990; Van den Bergen et al 1994) or electrochemical detection (Tang, Miles 2012). It has the advantage that (*1*) the *concentrations* can be determined, (*2*) applications are possible in the presence of inhibitors which interfere with the Q-electrode system, and (*3*) the ETS-reactive Q-pool can be distinguished from the inactive mtCoQ-pool. In the present study, we describe the Q-Module of the NextGen-O2k for real-time and simultaneous measurement of O_2 consumption and the redox state of the Q-mimetic CoQ_2 based on Rich (1988) and Moore et al (1988). The advantages of this technique are (*1*) real-time monitoring of continuous changes in the Q-redox state, and (*2*) sensitivity to the redox state of the ETS-reactive Q-pool without interference by inactive mtCoQ (Van den Bergen et al 1994).

2. Materials and methods

2.1. Reagents

ADP, adenosine 5'diphosphate potassium salt (Calbiochem 117105) stock 500 mM with 300 mM $MgCl_2$·6 H_2O: 501.3 mg ADP dissolved in 1.2 mL H_2O; pH neutralized with 5 M KOH; 122.0 mg $MgCl_2$·6 H_2O added, adjusted to pH 7.[#1]

Ama, antimycin A (Sigma Aldrich A8674) stock 5 mM: 5.4 mg dissolved in 2 mL EtOH.[#2]

CCCP, carbonyl cyanide 3-chlorophenylhydrazone carbonate (Sigma Aldrich C2759) stock 1 mM: 1.02 mg CCCP dissolved in 5 mL EtOH[#2]

CoQ_2 (Sigma Aldrich C8081) stock 10 mM: commercial vial (2 mg CoQ_2) dissolved in 628 µL EtOH. Stock 1 mM: 50 µL of 10 mM CoQ_2 stock diluted with 450 µL EtOH.[#2]

M, malate (Sigma Aldrich M1000) stock 400 mM: 268.2 mg dissolved in 3 mL H_2O, pH adjusted to 7.0 with 5 M KOH, volume adjusted to 5 mL.[#1]

P, pyruvate (Sigma Aldrich P2256) stock 2 M: 44 mg dissolved in 180 µL H_2O every day fresh.

Rot, rotenone (Sigma Aldrich R8875) stock 1 mM: 0.39 mg dissolved in 1 mL EtOH.[#2]

S, succinate (Sigma Aldrich S2378) stock 1 M: 1.351 g dissolved in 3 mL H_2O, pH adjusted to 7.0 with 1 M HCl, final volume adjusted to 5 mL.[#1]

Suspension buffer: 10.25 g mannitol (225 mM), 6.42 g sucrose (75 mM) and 0.095 g EGTA (1 mM) dissolved in 250 mL H_2O. pH adjusted to 7.4 with KOH or HCl if needed.[#1]

Isolation buffer A: 62.5 mg fatty acid free BSA (2.5 g/L) dissolved in 25 mL suspension buffer fresh every day.

Isolation buffer B: 5 mg subtilisin dissolved in 10 mL isolation buffer A, fresh every day.

Isolation buffer C: 0.25 g fatty acid free BSA (2.5 g/L) dissolved in 500 mL isolation buffer D every day freshly.

Isolation buffer D: 27.4 g sucrose (320 mM), 0.303 g Tris-Cl (10 mM), 0.093 g K-EDTA (1 mM) dissolved in 250 mL H_2O, pH adjusted to 7.4 with KOH or HCl if needed.[#1]

MiR05, mitochondrial respiration medium (Gnaiger et al 2000): 0.5 mM EGTA, 3 mM $MgCl_2$·$6H_2O$, 60 mM lactobionic acid, 20 mM taurine, 10 mM KH_2PO_4, 20 mM 2-[4-

(2-hydroxyethyl)piperazin-1-yl]ethanesulfonic acid HEPES, 110 mM sucrose, 1 g/L BSA; pH 7.1; prepared using MiR05-Kit (Oroboros Instruments, Austria 60101-01) and BSA.[#1]

[#1] Aliquots stored at -20 °C in plastic vials.

[#2] Aliquots stored at -20 °C in dark glass vials.

Further reagents were obtained from Sigma Aldrich (cat. Nº): MES, 2-(*N*-morpholino)ethanesulfonic acid hydrate (M8250); ATP, adenosine 5'-triphosphate disodium salt hydrate (A2383); BSA, fatty acid-free bovine serum albumin (A6003); $CaCO_3$ (C4830); D-sucrose (S7903); dithiothreitol (D0632); EGTA, ethylene glycol tetra acetic acid (E4378); imidazole (56750); KCl (60130); KH_2PO_4 (P5655); KOH (P1767); mannitol (M4125); phosphocreatine disodium salt (P7936); subtilisin, protease from *Bacillus licheniformis* Type VIII, lyophilized powders, 7-15 mg/unit (P5380). Bartelt, Austria: EtOH, ethanol 99.9 %, (CL0005055000); Scharlab: $MgCl_2{\cdot}6H_2O$ magnesium chloride hexahydrate (MA0036); Evoqua Water Technologies GmbH: H_2O, deionized ultra-pure water (Ultra Clear™ TP UV UF TM).

2.2. Animals

C57BL/6N wild-type young adult mice (male and female) were housed in clear plastic cages (maximum five mice per cage) in the animal facility of the Medical University of Innsbruck. Mice were kept in a controlled environment (23 ± 3 °C, 12/12 h light/dark cycle) and fed *ad libitum* with free access to water. After cervical dislocation, heart and brain were removed and immediately placed in ice-cold BIOPS. All procedures involving animals were conducted in accordance with the Austrian Animal Experimentation Act in compliance with the European convention for the protection of vertebrate animals used for experimental and other scientific purposes (Tierversuchsgesetz 2012; Directive 2010/63/EU; BMWFM-66.011/0128-WF/V/3b/2016). According to the 3Rs principle the number of animals was minimized.

2.3. Isolation of mitochondria

A glass/Teflon Potter-Elvehjem homogenizer (WiseStir HS-30E, Wisd laboratory instruments) and centrifuge (Rotina 380R, Andreas Hettich GmbH & Co. KG, Tuttlingen, Germany) were used. All procedures were carried out in an ice bath or at 4 °C.

Mouse heart mitochondria were isolated following Fontana-Ayoub et al (2015). Briefly, wet mass of the whole heart was determined, washed with ice-cold BIOPS and minced with scissors in ice-cold BIOPS (1 mL). The tissue was transferred into a pre-cooled glass/Teflon potter and homogenized at ~1000 rpm (five strokes) in 2 mL isolation buffer B. The homogenate was transferred to a 50-mL Falcon tube containing 3 mL isolation buffer B and centrifuged at 800 *g* for 10 min. Using a new 50-mL Falcon tube, the supernatant was centrifuged at 10 000 *g* for 10 min. The supernatant was discarded, the pellet was resuspended in isolation buffer A (final volume 2 mL), and centrifuged at 10 000 *g* for 10 min. The supernatant was discarded, and the mitochondrial pellet was finally resuspended in 200 µL suspension buffer.

Mouse brain mitochondria were isolated following Sumbalová et al (2016). Briefly, wet mass was determined, and the tissue was cut into small particles with sharp scissors in isolation buffer C. The medium was discarded, the tissue suspended in isolation buffer C (0.1 g tissue/1 mL), transferred to a pre-cooled glass/Teflon potter, and homogenized at 1000 rpm (five strokes). The homogenate was transferred to a 50-mL Falcon tube (0.5 g tissue/20 mL homogenate) and centrifuged at 1000 *g* for 10 min. The pellet was discarded, and the supernatant was centrifuged at 6200 *g* for 10 min. The supernatant was removed, the pellet resuspended in isolation buffer D (0.5 g tissue/10 mL), and recentrifuged at 6200 *g* for 10 min. The supernatant was discarded, and the mitochondrial pellet was finally suspended in 500 µL isolation buffer D.

The mitochondrial suspension was gently mixed with a 200-µL pipette (five up-down cycles), and 10 µL or 20 µL of heart or brain mitochondrial suspension was injected with a 50-µL Hamilton syringe into the O2k-chamber through the titration capillary of the stopper, respectively.

2.4. Mitochondrial protein content

Mitochondrial protein was determined based on Lowry et al (1951) using the DC™ Protein Assay (Bio-Rad, Hercules, CA, US) following the manufacturer instructions. The absorbance was measured at 620 nm in a Tecan Infinite TM F200 spectrophotometer (Tecan, Männedorf, Switzerland). 0.025 mg/mL isolated heart mitochondria and 0.09 mg/mL isolated brain mitochondria were applied in the experiments.

2.5. High-resolution respirometry

O_2 flux and the CoQ_2-redox states were measured in the NextGen-O2k (Oroboros Instruments, Austria), recorded, and analyzed using DatLab 7.4 (Oroboros Instruments, Austria). The O2k monitors the O_2 signal of polarographic oxygen sensors (POS) over time and plots O_2 consumption of a biological sample continuously. The two chambers of the O2k were calibrated at experimental volumes of 2 mL. Instrumental quality control was performed routinely as a standard operating procedure of HRR: (*1*) daily oxygen sensor test including air calibration in MiR05 at experimental temperature of 37 °C (stability ±0.002 °C), and stability of flux better than ±1 pmol·s^{-1}·mL^{-1}, and (*2*) monthly instrumental O_2 background test including zero calibration of the POS (Doerrier et al 2018; Gnaiger 2001; 2008). The medium was continuously stirred with a polyether ether ketone (PEEK)-coated magnetic stirrer bar at 750 rpm for optimum signal stability of the POS and mixing of the suspended sample and dissolved substances.

Volume-specific oxygen flux $J_{V,O2}$ [pmol·s^{-1}·mL^{-1}] was calculated real-time as the negative time derivative of the O_2 concentration by DatLab 7.4. The O_2 flux was corrected for (*1*) the instrumental O_2 background flux $J°_{O2}$, (*2*) dilution of the sample by titrations, and (*3*) residual oxygen consumption $J_{V,Rox}$ measured in the presence of isolated mitochondria without any respiratory fuel substrates and ADP or after inhibition of the electron transfer system.

2.6. Q-Module

The Q-Module of the NextGen-O2k provides the basis for continuous monitoring of the redox state of an added Q-mimetic in isolated mitochondria and chloroplasts (Figure 1). According to the original description (Rich 1988), a three-electrode system and a mobile short-chain Q-mimetic (CoQ_1 or CoQ_2) are required to indirectly detect the redox state of the ETS-reactive Q-pool trapped in the mitochondrial inner membrane mtIM. CoQ_2 reacts both with the biochemical sites of the ETS and the measuring electrode. Q-mimetics do not react directly with the long isoprenyl chain CoQ in the ETS, rather they are reduced by e.g. CI and CII, oxidized by CIII at the Q_o site and reduced at the Q_i site. If the redox state of the Q-mimetic is in equilibrium with the redox state of ETS-reactive CoQ, the redox state of the Q-mimetic reflects the redox state of ETS-reactive mtCoQ. In the present study, a low concentration of CoQ_2 (1 µM) was used, as described by Moore et al (1988; 1991).

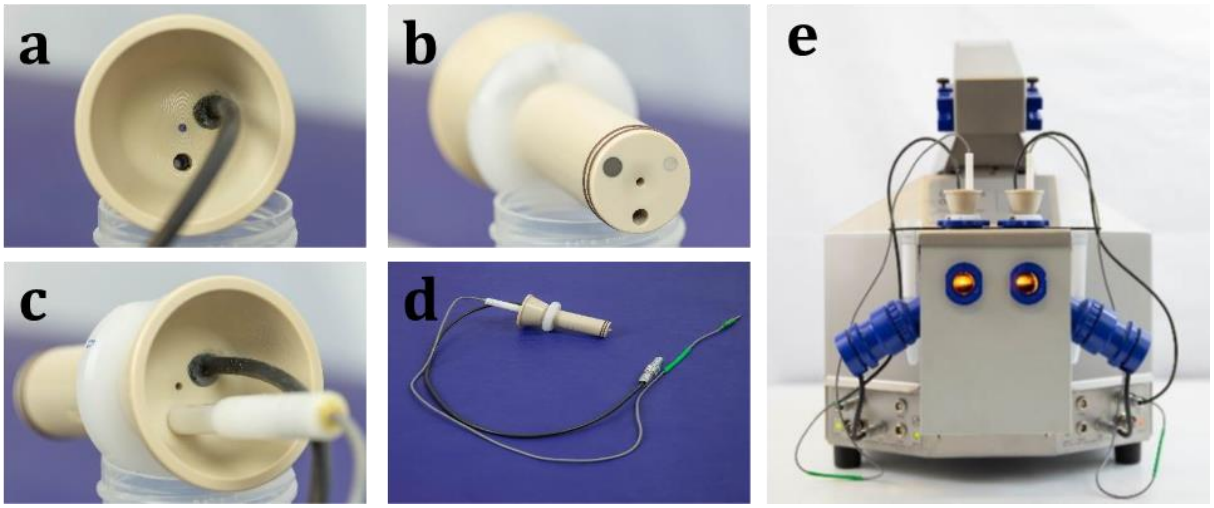

Figure 1. Q-Module with Q-sensor and stopper. The glassy carbon electrode (black) and platinum electrode (shiny silver) are built-in as fixed parts of the PEEK stopper. **(a)** Top view showing the central titration capillary and the inlet for the reference electrode (not inserted). **(b)** Bottom view with conical center guiding gas bubbles to the capillary, double Viton O-rings. **(c)** Top view with reference electrode. **(d)** Q-sensor with reference electrode. **(e)** Q-stopper inserted into the chamber of the NextGen-O2k prototype (front view).

The three-electrode system consists of a glassy carbon working electrode (GCE) set at a fixed potential relative to the silver/silver chloride (Ag/AgCl) reference electrode (Rich 1988). The potential set on the GCE is chosen to be sufficient to either oxidize the reduced or reduce the oxidized CoQ_2. A platinum (Pt) counter electrode completes the electronic circuit. If the GCE is set to a potential oxidizing CoQ_2, then CoQ_2 reduced by the ETS undergoes oxidation on the GCE surface, resulting in a current between the GCE and Pt electrode. This current [µA] was amplified by gain 100 and expressed in units [nA]. In this case the concentration of the reduced CoQ_2 is proportional to the current measured between GCE and Pt electrodes: the current increases in proportion to the concentration

of reduced CoQ_2. Conversely, if the GCE is set to the CoQ_2 reduction potential, the oxidized CoQ_2 undergoes reduction on the GCE surface and current flows into the opposite direction. In the present study, the GCE was set to the oxidation peak potential E_{p1} when measuring the CoQ_2 redox state. The GCE and Pt electrodes are built-in fixed parts of the Q-stopper, whereas the reference electrode can be inserted through a separate inlet (Figure 1).

2.7. Cyclic voltammetry

Cyclic voltammetry CV was controlled and recorded by DatLab 8.0 (Oroboros Instruments, Austria) before and after experiments. O2k-chambers were washed three times for 5 min with H_2O. In the meantime, the Q-sensor (Figure 1b) was polished with wetted 0.3 µm aluminum oxide powder on a polishing cloth, performing a figure eight motion in a vertical position 10-15 times, then polished with 0.05 µm aluminum powder in the same way. Afterwards, the Q-sensor and the separate reference electrode were rinsed with H_2O and wiped with a soft tissue (O2k-Manual: https://wiki.oroboros.at/index.php/MiPNet24.12_NextGen-O2k:_Q-Module).

After adding 2.3 mL MiR05 into the O2k-chamber, the Q-stopper was inserted with the mounted reference electrode into the O2k-chamber and excess medium was siphoned off the stopper receptacle. The background CV was determined without rotation of the stirrer. Then 30 µM CoQ_2 (6 µL of 10 mM stock) was titrated into the chamber and the stirrer switched on to mix the CoQ_2 solution. The stirrers were switched off and CV was started to determine the oxidation and reduction peak potentials of the Q-mimetic. Finally, the O2k-chamber, stopper, and reference electrode were washed with H_2O, 99.9 % EtOH, and H_2O again.

3. Results

3.1. Instrumental oxygen background test

The GC- and Pt-electrodes are fixed in the Q-stopper beside the titration capillary and a large capillary for inserting the reference electrode (Figure 1). The design was optimized for minimum O_2 diffusion through the stopper, comparable with the specifications of HRR using the standard O2k-stopper with a single injection capillary (Gnaiger 2001).

Correction for instrumental background O_2 flux is a standard procedure in HRR (Gnaiger 2001). The instrumental background O_2 flux is due to the O_2 consumption of the POS and O_2 diffusion into and out of the aqueous medium in the O2k-chamber, part of which may occur through diffusion leaks in the stopper. The instrumental background O_2 flux $J°_{O2}$ was measured in the absence of biological sample in the closed chamber in the range of experimental O_2 levels at four different O_2 concentrations: near air saturation ~170 µM, ~90 µM, ~45 µM, ~20 µM (Figure 2a). O_2 levels were reduced by dithionite titrations using the TIP2k (Titration-Injection microPump) and maintained for 20 min. O_2 flux was a linear function of O_2 concentration. The intercept ($a°$: flux at zero O_2 concentration) and slope ($b°$) were calculated from linear regressions for each individual

chamber. $a°$ was -2.6 ± 0.7 pmol·s^{-1}·mL^{-1} using the Q-stopper, not significantly different from the intercept measured with the regular O2k-stoppers (-2.3 ± 0.4 pmol·s^{-1}·mL^{-1}; Figure 2b and c).

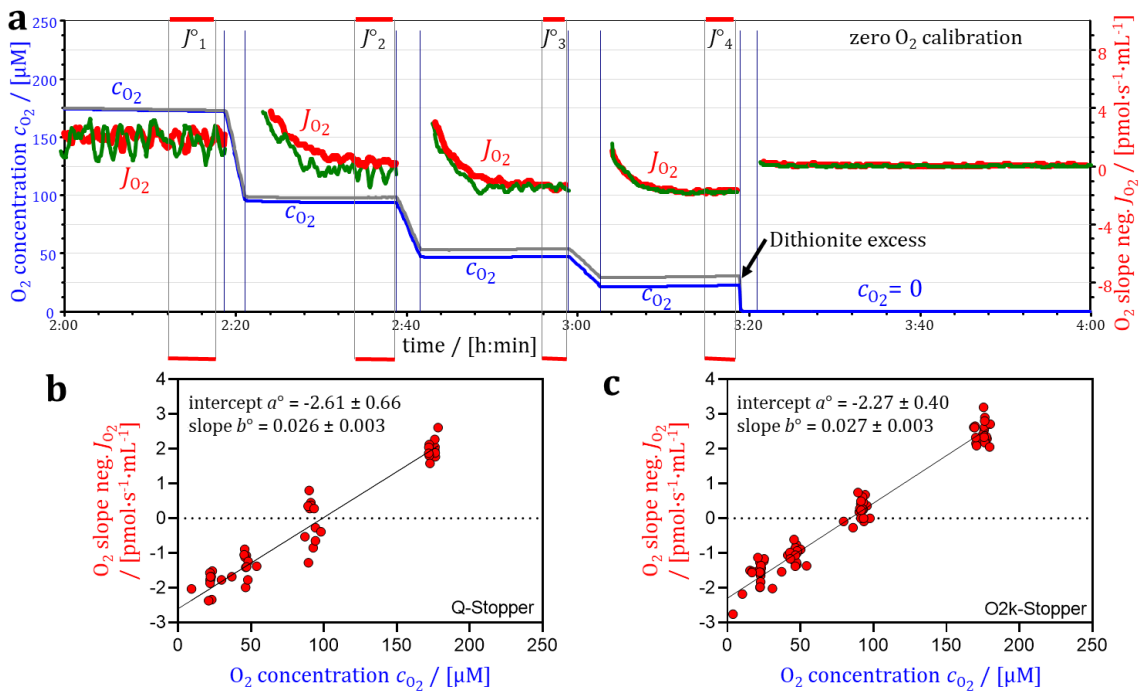

Figure 2. Instrumental O_2 background flux as a function of O_2 concentration: NextGen-O2k with Q-stoppers and O2k with regular O2k-stoppers. (a) Superimposed traces in two 2-mL chambers with Q-stoppers. $J°_i$ to $J°_4$ refer to background O_2 flux monitored at sequentially lowered O_2 concentrations. Excess dithionite (100 µL) added to deplete O_2 for zero calibration of the POS. Experiment 2019-08-28_PQ1-01. **(b)** 12 O2k-chambers using different Q-stoppers. **(c)** 20 O2k-chambers with regular O2k-stoppers. Average ± SD for the intercept $a°$ and slope $b°$ of linear regressions for individual chambers. Lines show linear regressions calculated through all data points.

3.2. Cyclic voltammetry

Cyclic voltammetry CV is applied in studies of the redox chemistry of CoQ (Gulaboski et al 2016). We applied CV at experimental conditions as quality control to (*1*) determine the oxidation- and reduction-peak potentials of CoQ_2 under specific experimental conditions, (*2*) check the quality of the Q-sensor, and (*3*) test the interference of chemicals used in the HRR assay with the Q-sensor. In CV, the electrical potential between the GCE and the Ag/AgCl electrode is varied over time in cycles, while the current is recorded between the GC- and Pt-electrodes. The current is plotted as a function of the applied electrical potential in the cyclic voltammogram, where the characteristic peaks refer to the maximum rate of CoQ_2 oxidation (oxidation peak potential, E_{p1}) and the maximum rate of reduction (reduction peak potential, E_{p2}; Figure 3). These values are set automatically by DatLab 8.0 and used to poise the GCE (Rich 1982; Rich 2004).

Figure 3 shows E_{p1} and E_{p2} determined after careful polishing of the GCE and Pt electrode using different Q-sensors in various chambers of the NextGen-O2k. The E_{p1} of CoQ_2 was 31.8 ± 6.5 mV, and E_{p2} was -269.9 ± 11.1 mV using freshly polished electrodes. Reproducibility of the CV measurements was high using different Q-sensors in various NextGen-O2k prototypes. In MiR05, 30 µM CoQ_2 was optimal for CV. Lower CoQ_2 concentrations did not result in detectable peaks, whereas the limit of detection was reached at higher than ~90 µM CoQ_2. The lowest concentration of CoQ_2 should be applied which gives well-defined E_{p1} and E_{p2}. Stirring of the solution is avoided during CV to minimize convection. Upon stirring in the presence of quinone (oxidized), only a peak related to quinone reduction is visible, whereas the peak of quinol oxidation cannot be observed, because the quinol is stirred off from the surface of GCE. At the start of CV an initial potential of +30 mV was used, which is close to the oxidation peak potential E_{p1} of CoQ_2. To avoid coating of the GCE, the initial potential must be close to the peak potential (Graham 2018). A polarization window was chosen of -500 mV to +500 mV versus Ag/AgCl. The narrowest possible range of potentials should be applied during CV scanning. Excessively high and low potentials might lead to chemical modification or coating of the GCE (Graham 2018). Coating of the GCE can inhibit electron transfer on the electrode surface.

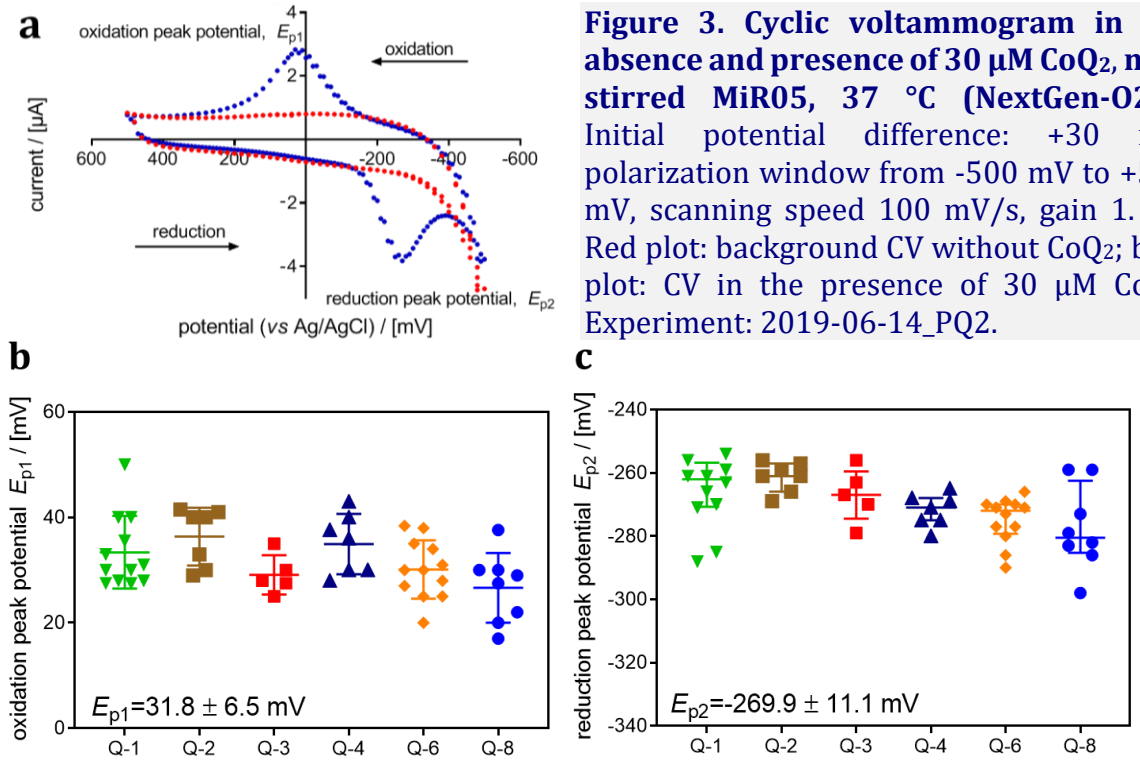

Figure 3. Cyclic voltammogram in the absence and presence of 30 µM CoQ_2, non-stirred MiR05, 37 °C (NextGen-O2k). Initial potential difference: +30 mV, polarization window from -500 mV to +500 mV, scanning speed 100 mV/s, gain 1. **(a)** Red plot: background CV without CoQ_2; blue plot: CV in the presence of 30 µM CoQ_2; Experiment: 2019-06-14_PQ2. **(b)** Oxidation peak potential E_{p1}, and **(c)** reduction peak potential E_{p2} of CoQ_2 with six different Q-sensors. E_{p1} and E_{p2} [mV] are shown as average ± SD; n=51.

We found an optimum of five cycles from -500 mV to +500 mV and back to -500 mV in standard CV applications. Although well-defined peaks for E_{p1} and E_{p2} were observed after one cycle, it is recommended to run more cycles to check whether additional peaks

are detected or the shape of E_{p1} and E_{p2} changes over the cycles owing to side-reactions. 100 mV/s was applied as scanning speed, which should allow for diffusion as the controlling process of exchange of CoQ_2 between the surface of GCE and the medium. If the scanning speed is very slow, CoQ_2 might be transported to and from the electrode surface by convection rather than diffusion. At too fast scanning speeds, the double layer charging current increases due to the rearrangement of solution molecules at the surface of the GCE. This results in high baseline currents that obscure the diffusion-controlled cyclic voltammogram (Graham 2018).

CV serves additionally as an essential quality control to evaluate the function of the Q-sensor, for minimizing directional long-term drift and non-directional short-term noise of the signal. No peaks should be observed in the background CV of complete incubation media without CoQ_2, while the peaks in the presence of 30 µM CoQ_2 should be well-defined and sufficiently sharp (Figure 3). If the peaks are not sharp enough and not well-defined, or additional peaks are observed (with and without CoQ_2), the GCE and Pt-electrode are polished with aluminum powder, the Q-sensor and O2k-chamber are washed with H_2O, 70 % EtOH, 99.9 % EtOH and H_2O, the glass barrel of the reference electrode is re-filled with 3 M KCl solution, and the quality of the porous vycor frit of the glass barrel of the reference electrode should be evaluated.

3.3. *Substrate-uncoupler-inhibitor titration protocols*

SUIT protocols are used to study respiratory control in different pathway- and coupling-control states in a single experimental assay. With a coupling-control protocol (SUIT-006 Q mt D071) and a coupling-pathway control protocol (SUIT-031 Q mt D072) we investigated O_2 flux and the redox state of the ETS-reactive Q-pool simultaneously (Figure 4 and 5). Harmonized SUIT protocols are applied with common cross-linked respiratory states, which can be considered as replicate measurements and therefore, allow harmonization of data obtained in different SUIT protocols. $S(Rot)_P$ and $S(Rot)_E$ are harmonized respiratory states in SUIT-006 and SUIT-031 without or with pyruvate & malate, respectively. In chemical background tests, titrations in the absence of mitochondria did not exert any effect on the Q-signal in both SUIT protocols.

The steps of coupling-control protocol SUIT-006 (Figure 4):

1. After addition of isolated mitochondria in the absence of fuel substrates and ADP, residual oxygen consumption with endogenous substrates *Ren* is due to oxidation of endogenous substrates that remained after mitochondrial isolation and residual O_2 consumption *Rox* not related to the ETS.
2. Addition of CoQ_2 (1 µM): residual endogenous respiration *Ren*.
3. Rotenone (Rot; 0.5 µM) and succinate (S; 10 mM): *Rox* after inhibition of respiration of endogenous substrates by Rot. Additionally, Rot prevents inhibition of succinate (S)-linked respiration caused by oxaloacetate accumulation (Gnaiger 2020). In the absence of rotenone, oxaloacetate is formed from malate in the reaction catalyzed by malate dehydrogenase MDH. Rot inhibits CI and oxidation of NADH, which results in an increase of the $NADH/NAD^+$ ratio and consequently to feed-back inhibition of MDH,

thus blocking formation of oxaloacetate. Succinate is formed in the tricarboxylic acid cycle and is the substrate of CII. It is oxidized to fumarate and supports electron transfer through CII to Q. Succinate with rotenone supports S-linked LEAK respiration and leads to reduction of CoQ_2, reflected in an increase of the Q-signal.

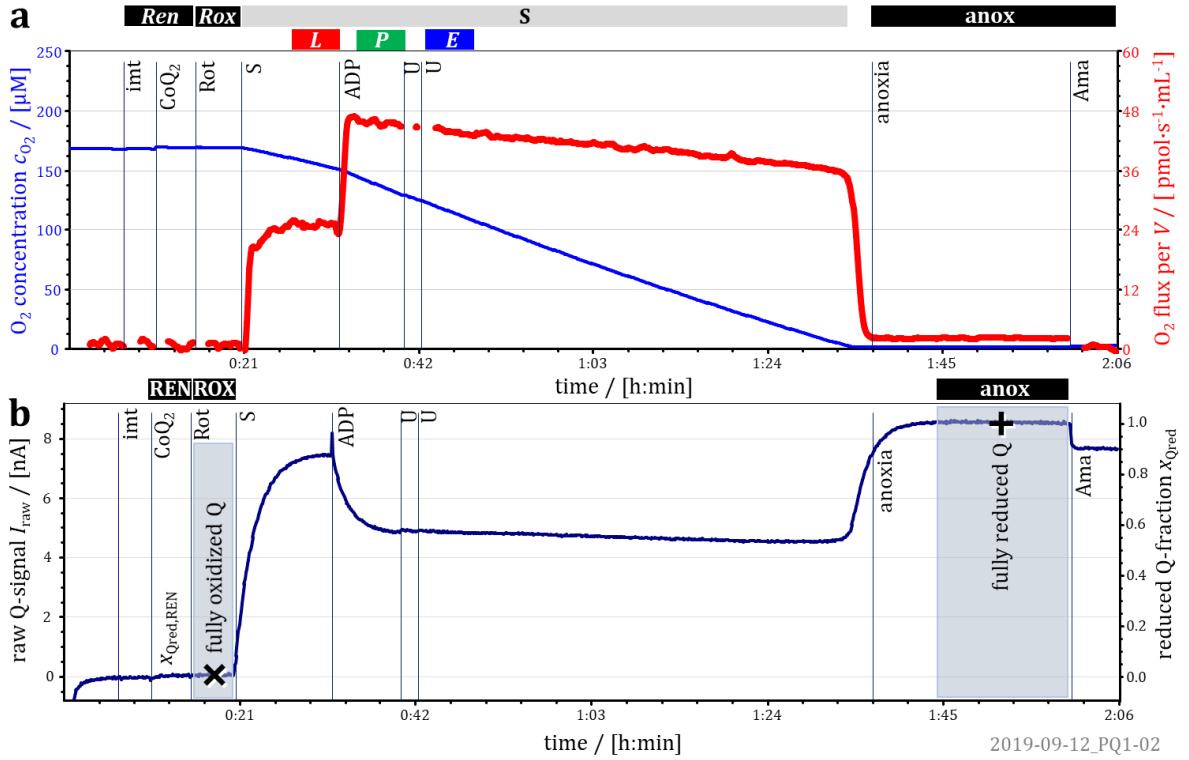

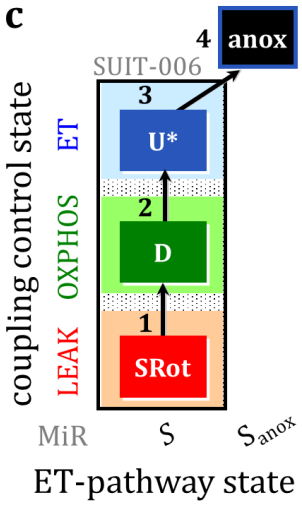

Figure 4. Coupling-control in the succinate-pathway S; SUIT-006. Simultaneous measurement of O_2 flux and redox state of the ETS-reactive Q-pool in mitochondria isolated from mouse heart. Simultaneous with SUIT-031 (Figure 5). **(a)** Blue plot: O_2 concentration [µM]; red plot: O_2 flux per volume [pmol·s^{-1}·mL^{-1}]. **(b)** Raw (non-calibrated) Q-signal I_{raw} [nA] and reduced Q-fraction x_{Qred}. *Ren* and *Rox*, residual oxygen consumption with endogenous substrates and after inhibition by rotenone (Rot) when fully oxidized CoQ_2 (x_{Qred} = 0) was calibrated (×). Further titrations: 1S, S-linked LEAK respiration *L*; 2D (ADP), S-linked OXPHOS capacity *P*; 3U (uncoupler CCCP; 1 µM), S-linked ET capacity *E*. Fully reduced CoQ_2 (x_{Qred} = 1) calibrated under anoxia (+). The effect of antimycin A (Ama) on the Q-signal was not due to the carrier EtOH. **(c)** Coupling/pathway control diagram.

4. ADP (D; 2.5 mM) was added at kinetically saturating concentration to stimulate S-OXPHOS capacity. A decrease of the Q-signal indicates partial oxidation of CoQ_2.
5. Uncoupler CCCP was titrated (U; 0.5 µM/step) after stimulation by ADP as a measure of electron transfer capacity *E*. Neither O_2 flux nor the Q-redox state changed after

CCCP titrations, showing that OXPHOS capacity was not limited by the phosphorylation system.

6. Anoxia was reached after the mitochondria consumed the O_2 in the O2k-chambers, the ETS and CoQ_2 become reduced. Anoxia was used for calibration of fully reduced Q (Section 3.4). Antimycin A (Ama; 2.5 µM) is a Q_i-site inhibitor of CIII and was added to check its effect on the fully reduced Q-pool under anoxia. The Q-signal in the presence of Ama did not show dependence on the O_2 concentration (data not shown).

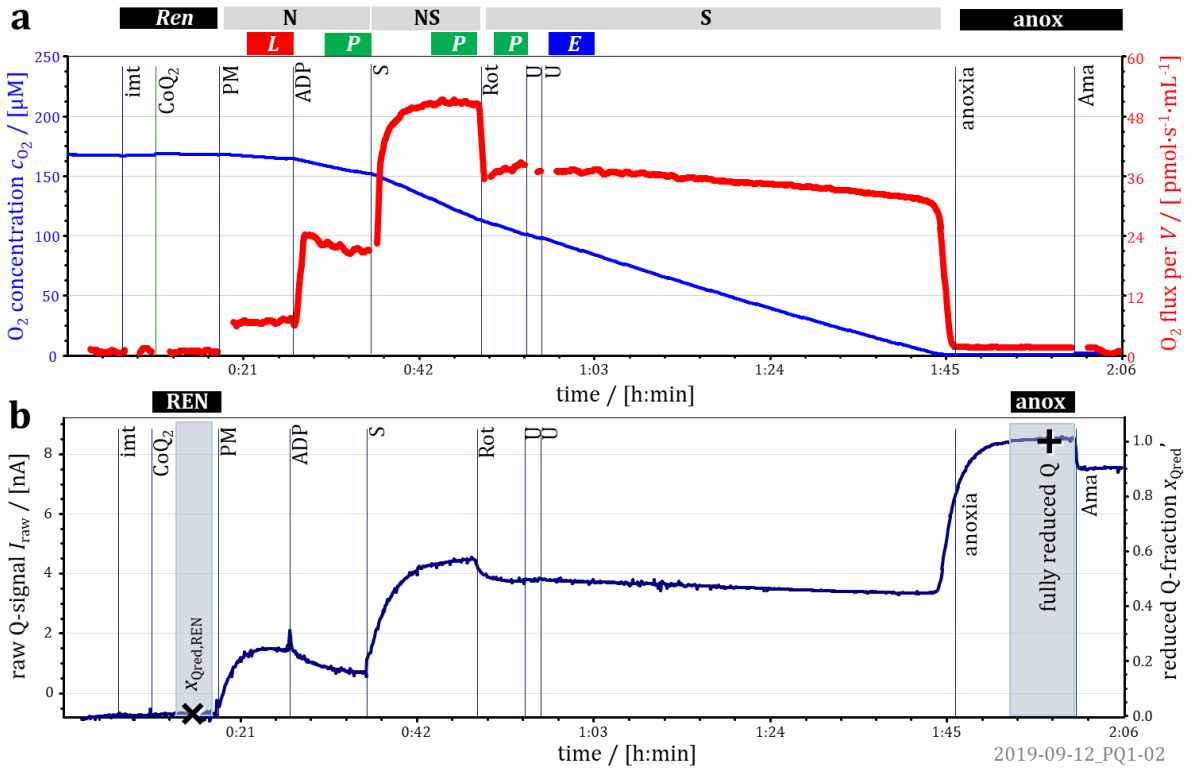

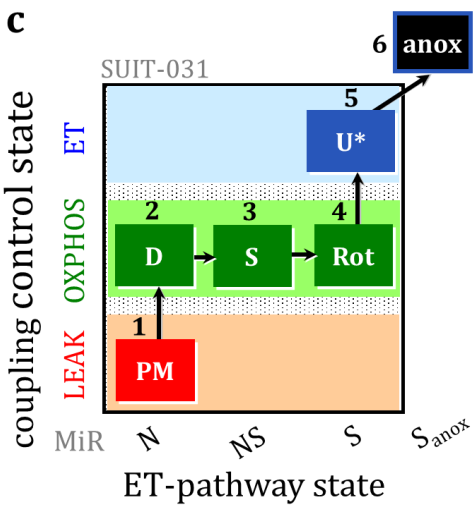

Figure 5. Pathway control in the N-, S-, and NS-pathways; SUIT-031. O_2 flux and redox state of the ETS-reactive Q-pool in mouse heart mitochondria. Simultaneous with SUIT-006 (Figure 4; see legend for abbreviations). **(a)** Blue plot: O_2 concentration [µM]; red plot: O_2 flux [pmol·s^{-1}·mL^{-1}]. **(b)** I_{raw} [nA] and apparent reduced Q-fraction x_{Qred}' with first calibration $x_{Qred,REN}$' = 0 in the state of residual endogenous respiration REN (×). Titrations: 1PM, N-linked LEAK respiration *L*; 2D, N-linked OXPHOS capacity *P*; 3S, NS-linked OXPHOS capacity *P*; 4Rot, S-linked OXPHOS capacity *P*; 5U (1 µM CCCP), S-linked ET capacity *E*. x_{Qred} = 1 calibrated under anoxia (+). **(c)** Coupling/pathway control diagram.

The steps of coupling-pathway control protocol SUIT-031 (Figure 5):

1. Addition of CoQ_2 (1 µM): residual endogenous respiration *Ren*.
2. Pyruvate & malate (PM; 5 mM P and 2 mM M) were added in immediate sequence to induce NADH-linked LEAK respiration. Pyruvate is converted to acetyl-CoA in the reaction catalyzed by pyruvate dehydrogenase. Malate serves as a co-substrate and after entering the mitochondria it is oxidized to oxaloacetate catalyzed by MDH. In both reactions NADH, the substrate of CI, is formed. Oxidation of NADH leads to reduction of the Q-pool through CI (Q-signal increased). PM caused only partial reduction of CoQ_2 in the LEAK state compared to S(Rot) in SUIT-006.
3. ADP (D; 2.5 mM) was added at kinetically saturating concentration to initiate N-OXPHOS capacity. A decrease of the Q-signal indicated partial oxidation of CoQ_2.
4. Succinate (S; 10 mM) was added to induce NS-convergent electron transfer. Succinate further increased the O_2 flux and reduced CoQ_2 in the OXPHOS state when added in the presence of PM, showing an additive effect in the Q-junction.
5. Rotenone (Rot; 0.5 µM) blocked N-linked respiration and led to oxidation of CoQ_2 via CI inhibition leading to S-OXPHOS. The two protocols are harmonized at state $S(Rot)_P$.
6. Uncoupler CCCP (U; 0.5 µM/step) was titrated (1 µM in total) to initiate S-ET capacity which is a common respiratory state to SUIT-006, $S(Rot)_E$. Neither O_2 flux nor the Q-redox state changed in mouse cardiac mitochondria showing that the S-OXPHOS capacity was not limited by the phosphorylation system.
7. Anoxia corresponds to the state where CoQ_2 is fully reduced (Section 3.4). Antimycin A (Ama; 2.5 µM).

3.4. Calibration: redox states of ETS-reactive Q

The redox state of ETS-reactive Q ($Q_{ra} \stackrel{def}{=} Q$) is expressed as the mole fraction (Cohen et al 2008) x_{Qred} of reduced Q in each steady state of a SUIT protocol. To calculate x_{Qred}, the raw CoQ_2 signal I_{raw} is calibrated against (*1*) the fully oxidized CoQ_2 signal I_{ox} and (*2*) the fully reduced CoQ_2 signal I_{red}. x_{Qred} is calculated as a fraction of fully reduced CoQ_2 (Table 1). The sum of the oxidized and reduced fractions of Q equals 1, $x_{Qred} + x_{Qox} = 1$. In this formalism the intermediate redox state of semiquinone is not taken into account.

I_{ox} is measured in the presence of CoQ_2 and isolated mitochondria, and absence of reduced fuel substrates. Isolated mitochondria may contain endogenous substrates which can slightly reduce Q_{ra} in the calibration state for I_{ox}. Then the CI inhibitor rotenone acting upstream of the Q-junction may inhibit respiration of endogenous substrates *Ren* further to *Rox* and decrease a small fraction of reduced Q in the REN state to the fully oxidized signal I_{ox} in the ROX state. The $x_{Qred,REN}$* calibrated against I_{ox} after rotenone addition in SUIT-006 (Figure 4) is used for correction of x_{Qred}' in SUIT-031 measured simultaneously in parallel O2k-chambers (Figure 5),

$$x_{Qred} = x_{Qred}' + x_{Qred,REN}^* \cdot (1 - x_{Qred}') \quad \text{Eq. 1}$$

Rotenone exerted no or a minor effect on mitochondrial respiration and the Q-signal when added after REN. The median $x_{Qred,REN}$* was 0.04 (range 0.03-0.05) in brain

mitochondria while respiration declined by 100 pmol·s^{-1}·mg^{-1} from *Ren* to *Rox*. The median $x_{Qred,REN}$* was 0.00 (range -0.01-0.01) in cardiac mitochondria without inhibitory effect of rotenone (*Ren* = *Rox*; Figure 4).

Table 1. Calculation of the reduced molar Q-fraction x_{Qred}. CoQ = UQ + USQ$^{\bullet-}$ + UQH_2

Symbol	Definition [Unit]	Quinol fraction x_{Qred}
I_{ox}	fully oxidized raw Q-signal [nA]	x_{Qred} = 0 (all CoQ is UQ)
I_{red}	fully reduced raw Q-signal [nA]	x_{Qred} = 1 (all CoQ is UQH_2)
I_{raw}	raw (non-calibrated) Q-signal [nA]	
x_{Qox} = 1	calibrated fully oxidized Q_{ra} fraction, quinone	$x_{Qred} = (I_{ox}-I_{ox})/(I_{red}-I_{ox}) = 0$
x_{Qred} =1	calibrated fully reduced Q_{ra} fraction, quinol	$x_{Qred} = (I_{red}-I_{ox})/(I_{red}-I_{ox}) = 1$
x_{Qred}	reduced Q_{ra} fraction	$x_{Qred} = (I_{raw}-I_{ox})/(I_{red}-I_{ox})$

The easiest and most accurate calibration of I_{red} at fully reduced Q_{ra} is performed under anoxia after mitochondria reduced the O_2 concentration practically to zero in the O2k-chamber with minimum O_2-backdiffusion (Figure 2). To do so, a mt-protein concentration >0.05 mg/mL is used which consumes relatively fast the O_2 in the closed chamber (Figure 4 and 5). Alternatively, the O_2 concentration can be decreased by nitrogen or hydrogen gas injection into the gas phase of an opened O2k-chamber, intermittently moving the stopper slightly upwards to form a gas phase above the stirred aqueous phase, and then allowing respiration to establish anoxia in the closed chamber.

3.5. Optimization of CoQ_2 concentration

The lowest practicable CoQ_2 concentration is applied to avoid side reactions on the ETS caused by the mimetic. 1 µM CoQ_2 was sufficient to detect the redox states of ETS-reactive Q (Figure 4 and 5), confirming previous studies (Moore et al 1991). This concentration of CoQ_2 did not influence respiration (Figure 6). It is recommended to test the effect of CoQ_2 on each type of mitochondria under experimental conditions. In the absence of CoQ_2 the raw Q-signal detected by the Q-sensor was ~11 % of the raw Q-signal detected with 1 µM CoQ_2 (Figure 7). At such a low signal, the drift becomes a confounding factor, emphasizing the need of adding a Q-mimetic. The Q-redox state did not differ when using 0.5-1.5 µM CoQ_2 measured at constant concentration of mouse heart mitochondria (Figure 8b).

3.6. Technical reproducibility

Figure 8a and b show x_{Qred} of technical replicates performed in parallel using different Q-sensors. In Figure 8a, the coupling-control protocol SUIT-006 (S-pathway) was applied in mouse brain mitochondria (representative trace: Figure 4).

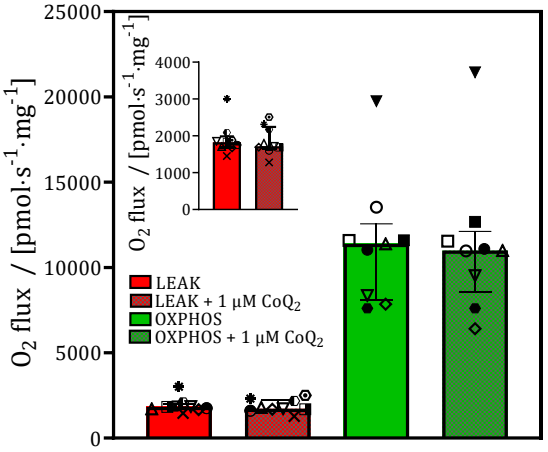

Figure 6. O_2 flux in the LEAK and OXPHOS states in the absence and presence of CoQ_2 (1 µM) in mitochondria isolated from mouse heart. Pyruvate (5 mM), glutamate (10 mM), malate (10 mM) and succinate (10 mM) were used to initiate LEAK respiration and kinetically saturating concentration of ADP (2.5 mM) was titrated to measure OXPHOS-capacity. Identical symbols are data from the same experimental day. Bars represent medians and interquartile ranges. The inset shows LEAK respiration expanded for better resolution.

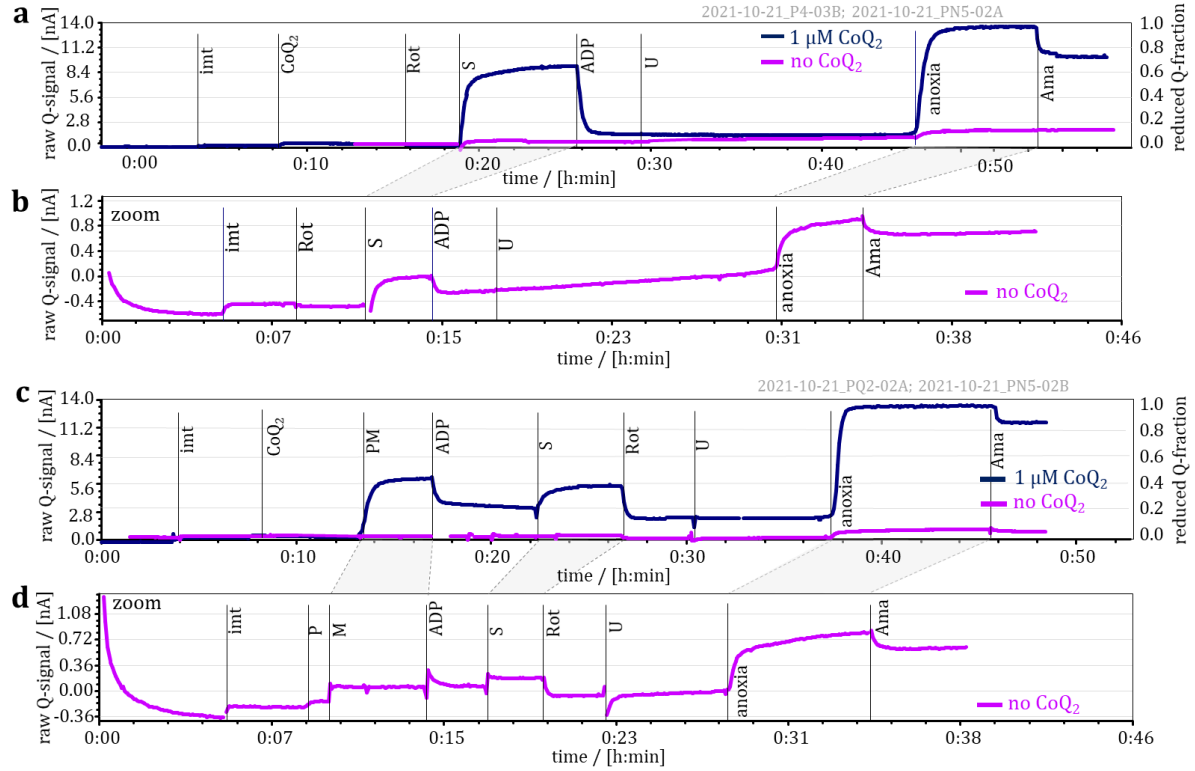

Figure 7. Raw Q-signal measured in the presence and absence of the Q-mimetic CoQ_2. imt: isolated mitochondria from mouse brain. **a** and **b:** SUIT-006, **c** and **d:** SUIT-031. Panels **b** and **d** are zooms into panels **a** and **c**, respectively. Rot rotenone; S succinate; U uncoupler (CCCP 1 µM); Ama antimycin A; PM pyruvate & malate.

In Figure 8b, both SUIT protocols (S- and N-pathways; representative traces: Figure 4 and 5) were used with mouse heart mitochondria. The results indicate a high reproducibility in every pathway- and coupling- control state. A range of CoQ_2 concentrations from 0.5 µM to 1.5 µM — at constant sample concentration — did not impact the redox state of the ETS-reactive Q-pool (Figure 8).

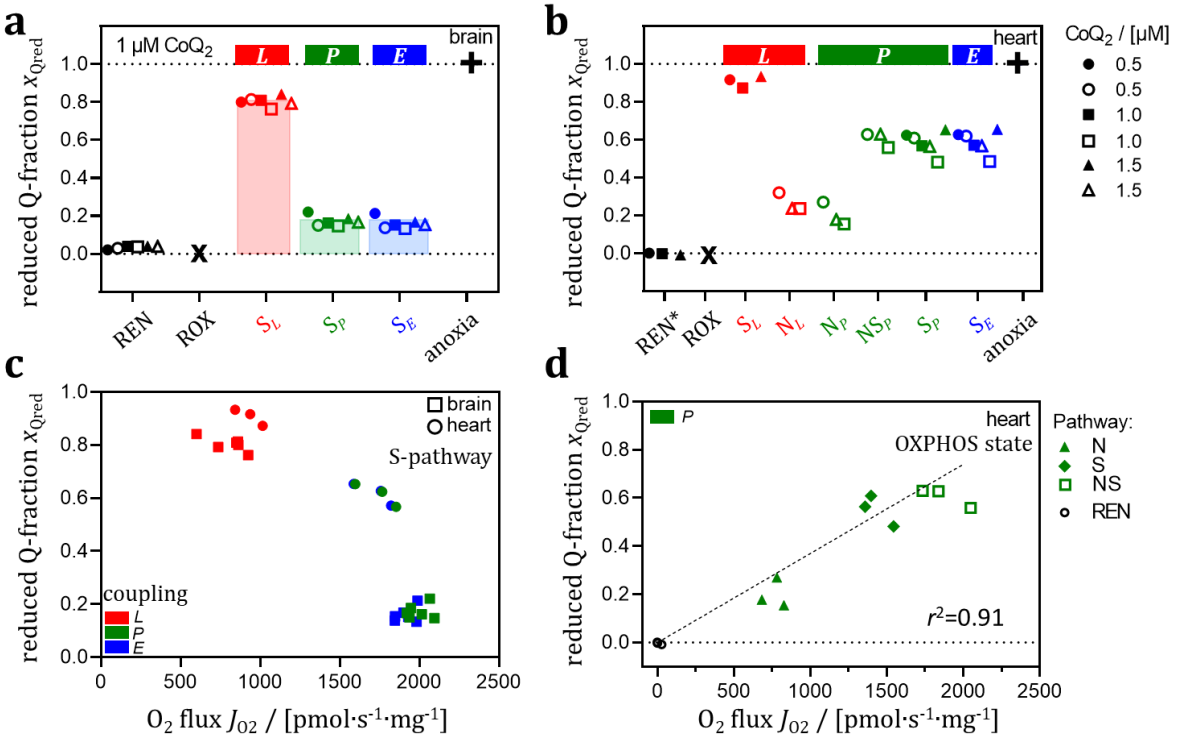

Figure 8. Reduced Q-fraction x_{Qred} and O_2 flux in mouse brain and heart mitochondria using six different Q-sensors. (a) Brain; SUIT-006; 1 µM CoQ_2. Fully oxidized Q (x_{Qred} = 0) calibrated in the presence of rotenone (×). Respiratory states: Residual endogenous respiration REN; residual oxygen consumption after addition of rotenone ROX; S-linked LEAK respiration S_L; S-linked OXPHOS capacity S_P; S-linked ET capacity S_E. Calibration of fully reduced Q (x_{Qred} = 1) under anoxia (+). Experiments: 2020-04-23_PN1-02; 2020-04-23_PN2-03; 2020-04-23_PQ2-02. **(b)** Heart; SUIT-006 (filled symbols) and SUIT-031 (open symbols); CoQ_2 concentrations as indicated. REN* from SUIT-006 used to correct fully oxidized Q (x_{Qred} = 0) in SUIT-031 (×). N-linked LEAK respiration N_L; N-linked OXPHOS capacity N_P; NS-linked OXPHOS capacity NS_P; S-linked OXPHOS capacity after inhibition by rotenone S_P; S-linked ET capacity S_E. Calibration of fully reduced Q (x_{Qred} = 1) under anoxia (+). **(c)** Coupling control: effect of increased load — from LEAK- to OXPHOS- and ET-states — on x_{Qred} as a function of O_2 flux per protein mass J_{O2} [pmol·s^{-1}·mg^{-1}] at constant S-pathway state (from panels **a** and **b**). **(d)** Pathway control: effect of increased drive — with electron input into the Q-junction by separate or combined convergent pathways — on x_{Qred} as a function of J_{O2} [pmol·s^{-1}·mg^{-1}] at constant OXPHOS-coupling state (from panel **b**). Inverted regression analysis was performed (Gnaiger 2021).

The raw Q-signal (current) at fully reduced CoQ_2 (I_{red}) ranged from 1.7 to 8.5 nA at CoQ_2 concentrations from 0.5 to 1.5 µM and mitochondria isolated from mouse brain or heart (Table 2). Variability between Q-sensors was similar to variability for individual Q-sensors, which might be caused by polishing of the Q-sensors before each experiment. This emphasizes the necessity for calibration of the Q-signal for I_{ox} and I_{red}.

Table 2. Variability of the raw Q-signal at the calibration points I_{ox} and I_{red} using different Q-sensors with mitochondria isolated from (a) mouse brain and (b) mouse heart at different concentrations of CoQ_2. I_{ox} calibrated in the ROX state (rotenone) or REN state (endogenous substrates) [#].

	[CoQ_2] µM	I_{ox} nA	I_{red} nA	I_{red} -I_{ox} nA	Q-sensor	DLD file Date O2k Chamber A/B
a						
	1.0	-0.023	5.829	5.852	P18-1	2020-04-23 PQ2-02A
	1.0	-0.660	3.790	4.450	P18-2	2020-04-23 PN1-02A
	1.0	-0.980	3.812	4.792	P18-3	2020-04-23 PN1-02B
	1.0	-0.098	4.682	4.780	P18-4	2020-04-23 PN2-03A
	1.0	-0.098	7.999	8.097	P18-5	2020-04-23 PN2-03B
	1.0	0.100	8.114	8.014	P18-6	2020-04-23 PQ2-02B
b						
	0.5	0.026	8.525	8.499	P18-1	2019-09-12 PQ2-03A
	0.5	-0.685[#]	8.511	9.196	P18-6	2019-09-12 PQ2-03B
	1.0	-0.042	1.897	1.939	P18-4	2019-09-12 PQ1-02A
	1.0	-0.066[#]	1.685	1.751	P18-5	2019-09-12 PQ1-02B
	1.5	-1.616	4.194	5.810	P18-2	2019-09-12 PQ3-02A
	1.5	-1.000[#]	3.333	4.333	P18-3	2019-09-12 PQ3-02B

3.7. Oxygen flux, reduced molar Q-fraction, and additivity

In the S-linked LEAK state, CoQ_2 was highly reduced in brain (x_{Qred} = 0.80; range 0.78 to 0.82) and heart (x_{Qred} = 0.92; 0.89 and 0.95; Figure 8a and b). In contrast, x_{Qred} was lower (less reduced) in the N-linked LEAK state (x_{Qred} = 0.24; 0.22 to 0.28; Figure 8b).

ADP-induced stimulation of respiration increases the load on the ETS. Under these conditions of increasing the load from the LEAK to OXPHOS state, CoQ_2 became more oxidized in brain (x_{Qred} = 0.16; range 0.13 to 0.19) and heart (x_{Qred} = 0.62; range 0.58 and 0.66; Figure 8c). In heart, x_{Qred} was higher in the S-linked (x_{Qred}=0.56; range 0.51 to 0.61) than in the N-linked (x_{Qred}=0.18; range 0.13 to 0.23) OXPHOS state (Figure 8b and d). This is consistent with the high ET-capacity of the S- compared to the N-pathway (Figure 5).

The higher electron supply capacity of the S-branch drives Q into a more reduced state. Uncoupler titrations (ET state) after stimulation by a kinetically saturating ADP concentration (OXPHOS state) did not affect respiration and Q-redox state in brain and heart, indicating that OXPHOS capacity is not limited by the capacity of the

phosphorylation system in these mitochondria (Gnaiger et al 2020). Whereas coupling control decreased x_{Qred} (more oxidized) by increasing the load (higher flux; Figure 8c), pathway control increases x_{Qred} (more reduced) by increasing the drive of electron input into the Q-junction (higher flux; Figure 8d).

OXPHOS capacity in heart mitochondria was low in the N-pathway (CI-linked) J_N = 780 (range 720 to 840) pmol·s^{-1}·mg^{-1}, higher in the S-pathway (CII-linked) J_S = 1397 (range 1317 to 1477) pmol·s^{-1}·mg^{-1} and showed an additive effect in the combined NS-pathway J_{NS} = 1837 (range 1706 to 1968) pmol·s^{-1}·mg^{-1}. The NS-linked O_2 flux (J_{NS}), however, was lower than $J_N + J_S$, demonstrating incomplete additivity. S was the dominant α-pathway with $J_S > J_N$. Then flux control ratios are $\alpha = J_S/J_{NS}$ and $\beta = J_N/J_{NS}$. Additivity $A_{\widetilde{\alpha\beta}}$ is defined as $(1 - \alpha)/\beta$ (Gnaiger 2020). Complete additivity ($A_{\widetilde{\alpha\beta}} = 1$) is obtained when the linear sum of the component N- and S-pathway ET capacities ($J_N + J_S$) equals the ET capacity of the convergent NS-pathway with the NS-substrate combination (J_{NS}). In heart, $A_{\widetilde{\alpha\beta}}$ was 0.57 (range 0.54 to 0.60) indicating incomplete NS-additivity of O_2 flux.

x_{Qred} was directly proportional to the OXPHOS capacity under pathway control — increasing from 0.18 (range 0.13 to 0.23) for N, 0.56 (range: 0.51 and 0.61) for S, to 0.63 (range 0.6 and 0.66) for NS — resulting in a linear dependence of x_{Qred} on respiratory rate. Proportionality — i.e. linearity and zero intercept — between reduction of CoQ_2 and ET capacities (N- and S-pathway) indicates that CoQ_2 equilibrates equally with the CI-Q-CIII and CII-Q-CIII branches of the electron transfer system and thus reflects the redox state of the ETS-reactive Q-pool (Table 3).

Table 3. Q-pools and redox-reactivity with the Q-mimetic CoQ_2

Q-pool	Symbol	Definition (CoQ_2: reactive or non-reactive)
coenzyme Q	CoQ	total CoQ in the cell, in mt-preparations, or added experimentally
mitochondrial CoQ	mtCoQ	total CoQ in mitochondria; mtCoQ = Q_{ra} + $mtCoQ_{ia}$
inactive mtCoQ	$mtCoQ_{ia}$	insensitive to changes in mitochondrial respiratory states; partially oxidized under anoxia and partially reduced in aerobic mt-preparations incubated without fuel substrates; (CoQ_2: non-reactive)
ETS-reactive Q	$Q_{ra} \stackrel{def}{=} Q$	fully reduced under anoxia, fully oxidized in aerobic mt-preparations incubated without external and internal fuel substrates and/or addition of inhibitors upstream of Q; Q = Q_{free} + Q_{SC}; (CoQ_2: reactive or possibly partially reactive)
free Q	Q_{free}	free pool of ETS-reactive Q according to the fluid-state model (random-collision model); (CoQ_2: reactive)
supercomplexed Q	Q_{SC}	pool of Q_{ra} bound to supercomplexes according to the solid-state model, not equilibrated with Q_{free}; (CoQ_2: reactive or possibly partially reactive)

4. Discussion

Evidence within the literature suggests that a large fraction of CI is organized as a supercomplex in conjunction with CIII and CIV (respirasome) contributing to the supercomplex-bound Q-pool Q_{SC}, whereas CII is not organized in a supercomplex but reacts with the free Q-pool Q_{free} according to the fluid-state model (Enriquez, Lenaz 2014). Even Q_{free} may not be homogenous, with central localization of ubiquinone in the lipid bilayer and more extensive interaction of ubiquinol with the peripheral phospholipid acyl chains (Ausili et al 2008). A direct link can be made between supercomplex channeling, interaction with the free Q-pool, and additivity of respiratory NS-pathway capacity. Complete channeling through the supercomplex $SCI_nIII_nIV_n$ predicts complete additivity ($A_{\widetilde{\alpha\beta}}$ = 1; Gnaiger 2020). Without interaction between the redox components in the channel and the free redox intermediates, there is no interaction between the N- and S-pathways which implies complete additivity. Importantly, the apparent excess capacity of CIV over the combined NS-ET capacity is high in mouse heart mitochondria (Lemieux et al 2017). Therefore, incomplete NS-additivity was not due to limitation of ET capacity downstream of Q.

In the present work we optimized the simultaneous measurement of the redox state of the ETS-reactive Q-pool and respiration in isolated mitochondria using the amperometric three-electrode sensor.

4.1. Advantages

Real-time and continuous detection of redox state: Monitoring the redox state of the ETS-reactive Q-pool in real-time is one of the main advantages of the electrochemical Q-sensor in contrast to the Q-extraction method. The Q-Module of the NextGen-O2k yields a significantly higher signal-to-noise ratio and lower drift compared to the original Q-electrode system (Moore et al 1991).

Zero to 50 % of the total mtCoQ-pool is not ETS-reactive (Urban, Klingenberg 1969; Kröger, Klingenberg 1973b; Jørgensen et al 1985; Van den Bergen et al 1994). The ETS-inactive mtCoQ-pool does not interact with the ETS nor CoQ_2. Thus, redox changes reported by the electrochemical Q-sensor are related to respiratory activity (Table 3).

Simultaneous measurement of Q-redox state and O_2 flux: The Q-Module of the NextGen-O2k allows for simultaneous measurement of redox state of the ETS-reactive Q-pool and O_2 flux in a closed chamber. Multiple titrations can be carried out via the titration capillary of the specifically designed stopper, which closes the O2k-chamber.

Controlled O_2 concentrations and high resolution: Owing to the near air-tight experimental O2k-chamber, the O_2 concentration can be increased or decreased (between 0 and 1000 µM the POS gives a linear response), which allows measurement not only at air saturation, but also in hypoxic and hyperoxic ranges. Minimizing the O_2 diffusion is essential to obtain anoxic conditions for calibration of fully reduced Q. Using the original Q-electrode system (Rich 1988; Moore et al 1988; Dry et al 1989) resolution of the oxygen sensor was limited and O_2 diffusion into the closed chamber posed a problem. Therefore, high mitochondrial concentrations were required.

4.2. Limitations

Q-pool compartmentalization: CoQ_2 does not interact directly with free mtCoQ. However, provided that both CoQ_2 and Q_{ra} have the same relative rates of reaction with the quinone-reactive complexes, CI, CII and CIII, then both CoQ_2 and ETS-reactive Q of the mtCoQ-pool will follow the same redox transitions. However, Q-compartmentalization may occur between a free ETS-reactive Q-pool in the lipid phase of the mtIM behaving according to the liquid-state or random-collision model and a bound ETS-reactive Q-pool tightly associated with respiratory supercomplexes. Such possible compartmentalization of Q needs to be considered in the interpretation of the amperometric signal of the Q-Module. This is particularly important if dissociation of supercomplexes is under control of the *pmF* (Enriquez, Lenaz 2014). Then equilibration of CoQ_2 with compartmentalized ETS-reactive Q relates to different pool sizes in the LEAK state at high *pmF* and the OXPHOS- and ET-states at lower and very low *pmF*, respectively (Figure 8). Pool size of the free mobile Q should not matter. In this context it is interesting to note that uncoupler titrations inducing the transition from $S(Rot)_P$ to $S(Rot)_E$ did not affect the Q-redox state nor O_2 flux in the presence or absence of pyruvate & malate (Figures 4 and 5). Inaccessible ETS-reactive Q-sites — and therefore inaccessible CoQ_2 non-reactive sites — in e.g. supercomplexes, however, would not be reported by the monitored CoQ_2 redox state. Importantly, the reduced Q-fraction x_{Qred} increased linearly and proportionally with respiratory flux from N-pathway control involving the supercomplex $SCI_nIII_nIV_n$ to S-pathway control (Figure 8d), suggesting that CoQ_2 is similarly reactive with the CI-Q-CIII and CII-Q-CIII branches irrespective of heterogeneity of the ETS-reactive Q-pool (Table 3).

mtCoQ concentration: Electrochemical determination of mtCoQ concentration is not possible (however, see Petrova et al 2014). If total mtCoQ is of interest (ETS-inactive and ETS-reactive), Q-extraction is the method of choice (Zannoni, Moore 1990; Van den Bergen et al 1994). CoQ_2 may interact with non-mitochondrial redox-reactive CoQ-pools which may interfere with the Q-signal in crude isolated mitochondria.

Chemical interference: Some inhibitors and chemicals applied in HRR interfere and may even damage the Q-sensor. Dithionite, cytochrome *c* (Osakai et al 2019), ascorbate, TMPD (tetramethyl-p-phenylenediamine dihydrochloride), CIV inhibitors (i.e. potassium cyanide and azide) and cyclohexylammonium salts of some chemicals (e.g. glycerol-3-phosphate) interfered with the Q-signal. The alternative ubiquinol oxidase inhibitor benzohydroxamate and NADH cannot be applied with the Q-electrode (Van den Bergen et al 1994). Thus, it is advisable to perform a chemical background test in the absence of biological sample, and CV in the absence and presence of 30 µM CoQ_2. If the shape of the CV has changed or additional "peaks" in the current in CV are detectable, a non-interfering alternative working electrode potential can be selected, changing between an oxidizing potential (to remove electrochemical interference from an oxidant) or reducing potential (to remove electrochemical interference from a reductant).

4.3. Conclusions

Electrochemical monitoring of the redox state of the ETS-reactive Q-pool adds a further dimension to coupling- and pathway-control analysis of isolated mitochondria. The Q-Module of the NextGen-O2k enables real-time monitoring of redox changes of the ETS-reactive Q-pool without interference by the inactive mtCoQ-pool. The reduced Q-fraction declines with respiratory rate stimulated by coupling control from LEAK to OXPHOS and ET states, but increases with respiration controlled by N-, S-, and convergent NS-pathway capacities. This powerful approach expands studies in mitochondrial physiology providing a greater insight into the role and regulation of mitochondrial function in health and disease.

Abbreviations

$A_{\widetilde{\alpha\beta}}$	additivity; $A_{\widetilde{\alpha\beta}} = (1- \alpha)/\beta$
α	dominant *FCR*; $\alpha = J_S/J_{NS}$
Ama	antimycin A
β	sub-dominant *FCR*; $\beta = J_N/J_{NS}$
CCCP	carbonyl cyanide m-chlorophenyl hydrazone
CI to CIV	Complex I to Complex IV
CoQ	coenzyme Q; mtCoQ: mitochondrial coenzyme Q, all protonation and redox states
CV	cyclic voltammetry
E	electron transfer capacity, ET capacity
E_{p1}, E_{p2}	oxidation peak potential, reduction peak potential [mV]
ETS	electron transfer system
FCR	flux control ratio
GCE	glassy carbon electrode
HRR	high-resolution respirometry
imt	isolated mitochondria
J	pathway O_2 flux
L	LEAK respiration
M	malate
N	NADH-linked pathway
P	pyruvate
P	capacity of oxidative phosphorylation, OXPHOS capacity
POS	polarographic oxygen sensor
Q, Q_{ra}	mitochondrial ETS-reactive coenzyme Q
Ren	residual endogenous respiration; REN: state of *Ren*
Rot	rotenone
Rox	residual oxygen consumption; ROX: state of *Rox*
S	succinate
SUIT	substrate-uncoupler-inhibitor titration
U	uncoupler
UQ	ubiquinone, oxidized
UQH_2	ubiquinol, reduced
$USQ^{\bullet-}$	ubisemiquinone, free radical

Acknowledgements

The hardware and electronics of the NextGen-O2k Q-Module was developed in collaboration with Phillip Gradl and his team (WGT-Elektronik GmbH & Co KG). Lukas Gradl and Markus Haider (H-Tech) were our partners in software development (DatLab 7.4 and DatLab 8.0 CV-Module, respectively). We thank Marco Di Marcello for excellent technical support in chemical and buffer preparation, mitochondrial isolation, and maintenance of the NextGen-O2k, and Chris Donnelly for stimulating discussions. This

work was supported by project NextGen-O2k which has received funding from the European Union's Horizon 2020 research and innovation programme under grant agreement Nº 859770.

References

Aberg F, Appelkvist EL, Dallner G, Ernster L (1992) Disturbation and redox state of ubiquinones in rat and human tissues. Arch Biochem Biophys 295:230-4.

Alcázar-Fabra M, Navas P, Brea-Calvo G (2016) Coenzyme Q biosynthesis and its role in the respiratory chain structure. Biochim Biophys Acta 1857:1073-8.

Ausili A, Torrecillas A, Aranda F, de Godos A, Sánchez-Bautista S, Corbalán-García S, Gómez-Fernández JC (2008) Redox state of coenzyme Q_{10} determines its membrane localization. J Phys Chem B112:12696-702.

Awad AM, Bradley MC, Fernandez-Del-Rio L, Nag A, Tsui HS, Clarke CF (2018) Coenzyme Q_{10} deficiencies: pathways in yeast and humans. Essays Biochem 62:361-76.

Balaban RS, Nemoto S, Finkel T (2005) Mitochondria, oxidants, and aging. Cell 120(4):483-95.

Bentinger M, Brismar K, Dallner G (2007) The antioxidant role of coenzyme Q. Mitochondrion 7:S41-50.

Bentinger M, Tekle M, Dallner G (2010) Coenzyme Q-biosynthesis and functions. Biochem Biophys Res Commun 396:74-9.

Bianchi C, Fato R, Genova ML, Parenti Castelli F, Lenaz G (2003) Structural and functional organization of Complex I in the mitochondrial respiratory chain. Biofactors 18:3-9.

Bianchi C, Genova ML, Parenti Castelli G, Lenaz G (2004) The mitochondrial respiratory chain is partially organized in a supercomplex assembly: kinetic evidence using flux control analysis. J Biol Chem 279:36562-9.

Cohen ER, Cvitas T, Frey JG, Holmström B, Kuchitsu K, Marquardt R, Mills I, Pavese F, Quack M, Stohner J, Strauss HL, Takami M, Thor HL (2008) Quantities, Units and Symbols in Physical Chemistry. IUPAC Green Book 3rd Edition, 2nd Printing, IUPAC & RSC Publishing, Cambridge.

Cottingham IR, Moore AL (1983) Ubiquinone pool behaviour in plant mitochondria Biochim Biophys Acta 724:191-200.

Crane FL, Hatefi Y, Lester RL, Widmer C (1957) Isolation of a quinone from beef heart mitochondria. Biochim Biophys Acta 1000:362-3.

Crane FL, Widmer C, Lester RL, Hatefi Y, Fechner W (1959) Studies on the electron transport system: XV. Coenzyme Q (Q_{275}) and the succinoxidase activity of the electron transport particle. Biochim Biophys Acta 31:476-89.

Crane FL, Sun IL, Clark MG, Grebing C, Low H (1985) Transplasma-membrane redox systems in growth and development. Biochim Biophys Acta 811:233-64.

Crofts AR (2004) The cytochrome bc_1 complex: function in the context of structure. Annu Rev Physiol 66:689-733.

Doerrier C, Garcia-Souza LF, Krumschnabel G, Wohlfarter Y, Meszaros AT, Gnaiger E (2018) High-resolution FluoRespirometry and OXPHOS protocols for human cells, permeabilized fibers from small biopsies of muscle, and isolated mitochondria. Methods Mol Biol 1782:31-70.

Dry IB, Moore AL, Day DA, Wiskich JT (1989) Regulation of alternative pathway activity in plant mitochondria: nonlinear relationship between electron flux and the redox poise of the quinone pool. Arch Biochem Biophys 273:148-57.

Echtay KS, Winkler E, Klingenberg M (2000) Coenzyme Q is an obligatory cofactor for uncoupling protein function. Nature 408:609-13.

Enriquez JA, Lenaz G (2014) Coenzyme Q and the respiratory chain: coenzyme Q pool and mitochondrial supercomplexes. Mol Syndromol 5:119-40.

Ernster L, Lee IY, Norling B, Persson B (1969) Studies with ubiquinone-depleted submitochondrial particles. Essentiality of ubiquinone for the interaction of succinate dehydrogenase, NADH dehydrogenase, and cytochrome b. Eur J Biochem 9:299-310.

Estornell E, Fato R, Castelluccio C, Cavazzoni M, Parenti Castelli G, Lenaz G (1992) Saturation kinetics of coenzyme Q in NADH and succinate oxidation in beef heart mitochondria. FEBS Letters 311:107-9.

Fazakerley 1DJ, Chaudhuri R, Yang P, Maghzal GJ, Thomas KC, Krycer JR, Humphrey SJ, Parker BL, Fisher-Wellman KH, Meoli CC, Hoffman NJ, Diskin C, Burchfield JG, Cowley MJ, Kaplan W, Modrusan Z, Kolumam G, Yang JY, Chen DL, Samocha-Bonet D, Greenfield JR, Hoehn KL, Stocker R, James DE (2018) Mitochondrial CoQ deficiency is a common driver of mitochondrial oxidants and insulin resistance. Elife 7:32111.

Fontaine E, Ichas F, Bernardi P (1998) A ubiquinone-binding site regulates the mitochondrial permeability transition pore. J Biol Chem 273:25734-40.

Fontana-Ayoub M, Krumschnabel G (2015) Isolation of mouse heart mitochondria. Mitochondr Physiol Network 20.06:1-2.

Gille L, Nohl H (2000) The existence of a lysosomal redox chain and the role of ubiquinone. Arch Biochem Biophys 375:347-54.

Gnaiger E (2001) Bioenergetics at low oxygen: dependence of respiration and phosphorylation on oxygen and adenosine diphosphate supply. Respir Physiol 128:277-97.

Gnaiger E (2008) Polarographic oxygen sensors, the oxygraph and high-resolution respirometry to assess mitochondrial function. In: Mitochondrial Dysfunction in Drug-Induced Toxicity (Dykens JA, Will Y, eds) John Wiley & Sons, Inc, Hoboken, NJ:327-52.

Gnaiger E (2020) Mitochondrial pathways and respiratory control. An introduction to OXPHOS analysis. 5th ed. Bioenerg Commun 2020.2:112 pp. https://doi.org/10.26124/bec:2020-0002

Gnaiger E (2021) Bioenergetic cluster analysis – mitochondrial respiratory control in human fibroblasts. MitoFit Preprints 2021.8. doi:10.26124/mitofit:2021-0008

Gnaiger E et al - MitoEAGLE Task Group (2020) Mitochondrial physiology. Bioenerg Commun 2020.1:1-44. https://doi.org/10.26124/bec:2020-0001.v1

Gnaiger E, Kuznetsov AV, Schneeberger S, Seiler R, Brandacher G, Steurer W, Margreiter R (2000) Mitochondria in the cold. In: Life in the Cold (Heldmaier G, Klingenspor M, eds) Springer, Heidelberg, Berlin, New York:431-42.

Goldstein JL, Brown MS (1990) Regulation of the mevalonate pathway. Nature 343:425-30.

González-Mariscal I, García-Testón E, Padilla S, Martín-Montalvo A, Pomares-Viciana T, Vazquez-Fonseca L, Gandolfo-Domínguez P, Santos-Ocaña C (2014) Regulation of coenzyme Q biosynthesis in yeast: a new complex in the block. IUBMB Life 66:63-70.

Graham DJ (2018) Standard operating procedures for cyclic voltammetry. 126 pp. ISBN: 978-1387514304.

Gulaboski R, Markovski V, Jihe Z (2016) Redox chemistry of coenzyme Q—a short overview of the voltammetric features. J Solid State Electrochem 20:3229–3238.

Gutman M (1985) Kinetic Analysis of electron flux through the mitochondrial system. Coenzyme Q, Chichester, UK: Wiley 10: 215-234.

Gvozdjáková A, Sumbalová Z, Kucharská J, Komlósi M, Rausová Z, Vančová O, Számošová M, Mojto V (2020) Platelet mitochondrial respiration, endogenous coenzyme Q_{10} and oxidative stress in patients with chronic kidney disease. Diagnostics (Basel) 10:176.

Gvozdjáková A, Sumbalová Z, Kucharská J, Szamosová M, Čápová L, Rausová Z, Vančová O, Mojto V, Langsjoen P, Palacka P (2021) Platelet mitochondrial respiration and coenzyme Q_{10} could be used as new diagnostic strategy for mitochondrial dysfunction in rheumatoid diseases. PLoS ONE 16:e0256135.

Hackenbrock CR, Chazotte B, Gupte SS (1986) The random collision model and a critical assessment of diffusion and collision in mitochondrial electron transport. J Bioenerg Biomembr 18:331–368.

Hatefi Y, Lester RL, Crane FL, Widmer C (1959) Studies on the electron transport system. XVI. Enzymic oxidoreduction reactions of coenzyme Q. Biochim Biophys Acta 31:490-501.

Hernández-Camacho JD, Bernier M, López-Lluch G, Navas P (2018) Coenzyme Q_{10} supplementation in aging and disease. Front Physiol 9:44.

Hunte C, Palsdottir H, Trumpower BL (2003) Protonmotive pathways and mechanisms in the cytochrome bc1 complex. FEBS Lett 545:39-46.

Jørgensen BM, Rasmussen HN, Rasmussen UF (1985) Ubiquinone reduction pattern in pigeon heart mitochondria. Identification of three distinct ubiquinone pools. Biochem J 229:621-9.

Kalén A, Appelkvist EL, Dallner G (1987) Biosynthesis of ubiquinone in rat liver. Acta Chem Scand B41:70-2.

Kröger A, Klingenberg M (1966) On the role of ubiquinone in mitochondria. II. Redox reactions of ubiquinone under the control of oxidative phosphorylation. Biochem Z 344:317-36.

Kröger A, Klingenberg M (1973a) The kinetics of the redox reactions of ubiquinone related to the electron-transport activity in the respiratory chain. Eur J Biochem 34: 358-68.

Kröger A, Klingenberg M (1973b) Further evidence for the pool function of ubiquinone as derived from the inhibition of the electron transport by antimycin. Eur J Biochem 39:313-23.

Lemieux H, Blier PU, Gnaiger E (2017) Remodeling pathway control of mitochondrial respiratory capacity by temperature in mouse heart: electron flow through the Q-junction in permeabilized fibers. Sci Rep 7:2840. doi:10.1038/s41598-017-02789-8

Lenaz G, Genova ML (2009) Structural and functional organization of the mitochondrial respiratory chain: A dynamic super-assembly. Int J Biochem Cell Biol 41:1750-72.

Lopez-Lluch G, Rodriguez-Aguilera JC, Santos-Ocana C, Navas P (2010) Is coenzyme Q a key factor in aging? Mech Ageing Dev 131:225-35.

Lowry OH, Rosebrough NJ, Farr AL, Randall RJ (1951) Protein measurement with the Folin phenol reagent. J Biol Chem 193:265-75.

Miles MV (2007) The uptake and distribution of coenzyme Q(10). Mitochondrion 7 Suppl:S72-7.

Mitchell P (1961) Coupling of phosphorylation to electron and hydrogen transfer by a chemi-osmotic type of mechanism. Nature 191:144-8.

Mitchell P (1975) The protonmotive Q cycle: A general formulation. FEBS Lett 59:137-9.

Moore AL, Dry IB, Wiskich TJ (1988) Measurement of the redox state of the ubiquinone pool in plant mitochondria. FEBS Lett 235:76-80.

Moore AL, Dry IB, Wiskich JT (1991) Regulation of electron transport in plant mitochondria under State 4 Conditions. Plant Physiol 95:34-40.

Morré DJ, Morré DM (1989) Preparation of mammalian plasma membranes by aqueous two-phase partition. Biotechniques 7:946-958.

Morré DJ, Morré DM (2011) Non-mitochondrial coenzyme Q. Biofactors 37:355-60.

Noh YH, Kim K-Y, Shim MS, Choi S-H, Choi S, Ellisman MH, Weinreb RN, Perkins GA, Ju W-K (2013) Inhibition of oxidative stress by coenzyme Q10 increases mitochondrial mass and improves bioenergetic function in optic nerve head astrocytes. Cell Death Dis 4:e820.

Nyquist SE, Barr R, Morré DJ (1970) Ubiquinone from rat liver Golgi apparatus fractions. Biochim Biophys Acta 208:532-4.

Osakai T, Yamamoto T, Ueki M (2019) Directional electron transfer from ubiquinone-10 to cytochrome c at a biomimetic self-assembled monolayer modified electrode. Electrochemistry 87:59-64.

Petrova EV, Korotkova EI, Kratochvil B, Voronova OA, Dorozhko EV, Bulycheva EV (2014) Investigation of coenzyme Q_{10} by voltammetry. Proc Chem 10:173-8.

Rauchová H, Fato R, Drahota Z, Lenaz G (1997) Steady-state kinetics of reduction of coenzyme Q analogs by glycerol-3-phosphate dehydrogenase in brown adipose tissue mitochondria. Arch Biochem Biophys 344:235-41.

Reed JS, Ragan CI (1987) The effect of rate limitation by cytochrome *c* on the redox state of the ubiquinone pool in reconstituted NADH: cytochrome *c* reductase. Biochem J 247:657-62.

Rich PR (1982) Electron and proton transfers in chemical and biological quinone systems. Faraday Discuss Chem Soc 74:349-64.

Rich PR (1984) Electron and proton transfers through quinones and cytochrome *bc* complexes. Biochim Biophys Acta 768:53-79.

Rich PR (1988) Patent of Q-electrode. Monitoring membrane bounded systems. Glynn Res. Ph., Bodmin; European Patent Nº85900699.1.

Rich PR (2004) The quinone chemistry of *bc* complexes. Biochim Biophys Acta 1658:165-71.

Rodríguez-Hernández A, Cordero MD, Salviati L, Artuch R, Pineda M, Briones P, Izquierdo LG, Cotán D, Navas P, Sánchez-Alcázar JA (2009) Coenzyme Q deficiency triggers mitochondria degradation by mitophagy. Autophagy 5:19-32.

Sastry PS, Jayaraman J, Ramasarma T (1961) Distribution of coenzyme Q in rat liver cell fractions. Nature 189:577.

Song Y, Buettner GR (2011) Thermodynamic and kinetic considerations for the reaction of semiquinone radicals to form superoxide and hydrogen peroxide. Free Radical Biol Med 919-62.

Stefely JA, Pagliarini DJ (2018) Biochemistry of mitochondrial coenzyme Q biosynthesis. Trends Biochem Sci 42: 824–43.

Stoner CD (1984) Steady-state kinetics of the overall oxidative phosphorylation reaction in heart mitochondria. Determination of the coupling relationships between the respiratory reactions and miscellaneous observations concerning rate-limiting steps. J Bioenerg Biomembr 16:115-41.

Sumbalová Z, Fontana M, Krumschnabel G (2016) Isolation of rat brain mitochondria. Mitochondr Physiol Network 20.07:1-2.

Takada M, Ikenoya S, Yuzuriha T, Katayama K (1984) Simultaneous determination of reduced and oxidized ubiquinones. Methods Enzymol 105:147-55.

Tang PH, Miles MV (2012) Measurement of oxidized and reduced coenzyme Q in biological fluids, cells, and tissues: an HPLC-EC method. Methods Mol Biol 837:149-68.

Tran UC, Clarke CF (2007) Endogenous synthesis of coenzyme Q in eukaryotes. Mitochondrion 7 Suppl:S62-71.

Trumpower BL (1990) The protonmotive Q cycle. Energy transduction by coupling of proton translocation to electron transfer by the cytochrome bc1 complex. J Biol Chem 265:11409-12.

Trumpower BL, Gennis RB (1994) Energy transduction by cytochrome complexes in mitochondrial and bacterial respiration: the enzymology of coupling electron transfer reactions to transmembrane proton translocation. Annu Rev Biochem 63:675-716.

Turunen M, Olsson J, Dallner G (2004) Metabolism and function of coenzyme Q. Biochim Biophys Acta 1660:171-99.

Urban PF, Klingenberg M (1969) On the redox potentials of ubiquinone and cytochrome b in the respiratory chain. Eur J Biochem 9:519-25.

Van den Bergen CW, Wagner AM, Krab K, Moore AL (1994) The relationship between electron flux and the redox poise of the quinone pool in plant mitochondria. Interplay between quinol-oxidizing and quinone-reducing pathways. Eur J Biochem 226:1071-8.

Watts JL, Ristow M (2017) Lipid and carbohydrate metabolism in *Caenorhabditis elegans*. Genetics 207:413-46.

Wolf DE, Hoffman CH, Trenner NR, Arison BH, Shunk CH, Linn BO, McPherson JF, Folkers K (1958) Coenzyme Q. I. Structure studies on the coenzyme Q group. J Am Chem Soc 80:4752.

Zannoni D, Moore AL (1990) Measurement of the redox state of the ubiquinone pool in *Rhodobacter capsulata* membrane fragments. FEBS Lett 271:123-7.

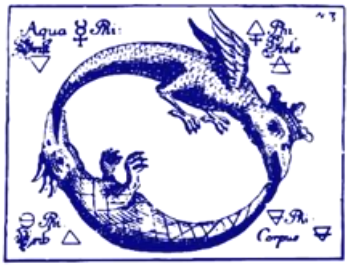

BIOENERGETICS COMMUNICATIONS